

Laser-induced alignment dynamics of HCN: Roles of the permanent dipole moment and the polarizability

Claude M. Dion,^{1,2} Arne Keller,¹ Osman Atabek,¹ and André D. Bandrauk²

¹*Laboratoire de Photophysique Moléculaire du Centre National de la Recherche Scientifique, Université Paris-Sud, Bâtiment 213, 91405 Orsay, France*

²*Laboratoire de Chimie Théorique, Faculté des Sciences, Université de Sherbrooke, Sherbrooke, Québec, Canada J1K 2R1*
(Received 13 May 1998)

The alignment dynamics of HCN, in a linear configuration, interacting with linearly polarized infrared laser pulses are studied numerically by exact (nonperturbative) solutions of the time-dependent Schrödinger equation. The alignment, with respect to the laser field polarization vector, is measured from the angular distribution of the molecule using a defined half angle $\theta_{1/2}$. It is shown that, at intensities $I=10^{13}$ W/cm², alignment can be achieved on a subpicosecond time scale with a single laser frequency, in the presence of simultaneous dipole- and polarizability-field interactions. The results are compared to those of a laser-driven rigid-rotor analytical model that is thoroughly developed. The importance of the permanent and field-induced dipole moments on the alignment process is investigated, as well as the role of vibrational excitation of the two molecular bonds. [S1050-2947(99)03302-8]

PACS number(s): 42.50.Hz, 33.80.-b

I. INTRODUCTION

The study of the interaction of molecules with intense laser fields is receiving increasing interest [1]. This has led to the discovery of nonlinear, nonperturbative effects such as above-threshold dissociation and laser-induced avoided crossings in high-intensity resonant electronic excitation. The previously observed anisotropy in the angular distribution of fragments in photodissociation experiments [2] has led to the study of laser-induced molecular alignment, with possible laser manipulations of molecules as a goal.

Alignment and orientation of molecules with respect to the laser electric field polarization vector can lead to an enhancement of detection signals in experiments and is useful in permitting reduced-dimension models in theoretical calculations [3]. It has been suggested as a tool to control laser-induced isomerization [4] and collisional cross sections in the study of chemical reactivity [5] or in femtochemistry experiments [6], to obtain separation of isotopes [7] or photofragments [8,9], to trap molecules [10,11], and to control laser-focused molecular beams [11,12] to achieve nanoscale design.

We propose to study the time-resolved alignment dynamics of polyatomic molecules from exact solutions of the time-dependent Schrödinger equation (TDSE) in intense infrared laser pulses. This work offers a complementary approach to previous studies that have concentrated essentially on photodissociation fragments [13] or time-averaged pendular states [10,14,15]. We shall examine the effect of polarizability, in addition to the permanent molecular dipole moment, on the alignment of molecules in a complete dynamical treatment that will include resonant and nonresonant internal excitations of a molecule such as HCN.

The first part of this paper is devoted to the theoretical quantum approach used in this study, as applied to the HCN molecule. This is complemented by an analytical laser-driven rigid-rotor model that puts the emphasis on the polarizability of the molecule and offers a simple interpretation when vibrational modes are not significantly active. It is fol-

lowed by a presentation of the numerical results obtained from the TDSE and the analysis of some of the observed alignment features. Finally, the conclusion gives some suggestions for further research and issues to be addressed in the nonperturbative regime of the laser-molecule interaction made available by current laser technology.

II. THEORY

A. Model

We will consider a linear HCN molecule, the intramolecular bending angle being kept fixed, as shown in Fig. 1. The complete molecule-plus-field Hamiltonian for this model is

$$\hat{H} = \hat{H}_R + \hat{H}_r + \hat{H}_{\text{rot}} + V(R, r) + \hat{H}_L, \quad (1)$$

with

$$\hat{H}_R = -\frac{\hbar^2}{2\mu_{\text{HCN}}} \frac{1}{R^2} \frac{\partial}{\partial R} \left(R^2 \frac{\partial}{\partial R} \right) \quad (2)$$

for the H to center of mass of CN coordinate and

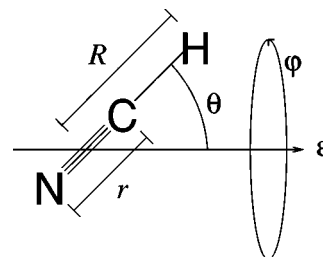


FIG. 1. Model used for HCN. R is the distance between H and the center of mass of CN; r is the CN bond length; θ and φ are, respectively, the polar and azimuthal angles of the molecular axis with respect to the laser field polarization vector.

TABLE I. Equilibrium values and derivatives of the dipole moment and the polarizability for the HCN molecule [4,18,19], in atomic units.

Equilibrium value	R derivative	r derivative
$\mu_0 = 1.137$	$\partial\mu_0/\partial R = 0.171$	$\partial\mu_0/\partial r = -0.175$
$\alpha_{\parallel} = 21.71$	$\partial\alpha_{\parallel}/\partial R = 6.51$	$\partial\alpha_{\parallel}/\partial r = 11.97$
$\alpha_{\perp} = 13.28$	$\partial\alpha_{\perp}/\partial R = 0.62$	$\partial\alpha_{\perp}/\partial r = 2.07$

$$\hat{H}_r = -\frac{\hbar^2}{2\mu_{\text{CN}}} \frac{1}{r^2} \frac{\partial}{\partial r} \left(r^2 \frac{\partial}{\partial r} \right) \quad (3)$$

for the $\text{C}\equiv\text{N}$ bond distance, μ_{HCN} and μ_{CN} being the reduced masses

$$\mu_{\text{HCN}} = \frac{m_{\text{H}}(m_{\text{C}} + m_{\text{N}})}{m_{\text{H}} + m_{\text{C}} + m_{\text{N}}}, \quad \mu_{\text{CN}} = \frac{m_{\text{C}}m_{\text{N}}}{m_{\text{C}} + m_{\text{N}}},$$

$$\begin{aligned} \hat{H}_{\text{rot}} &= \frac{\hbar^2 \hat{J}^2}{2I(R, r)} \\ &= \frac{\hbar^2}{2I(R, r)} \left[-\frac{1}{\sin \theta} \frac{\partial}{\partial \theta} \left(\sin \theta \frac{\partial}{\partial \theta} \right) - \frac{1}{\sin^2 \theta} \frac{\partial^2}{\partial \varphi^2} \right], \end{aligned} \quad (4)$$

with $I(R, r)$ the principal moment of inertia of the molecule, which defines the rotational constant $B = \hbar/4\pi c I$ (the equilibrium value is $B_0 = 1.478 \text{ cm}^{-1}$ for HCN [16]). The laser-molecule interaction is given by

$$\hat{H}_L = -\vec{\mu}(R, r) \cdot \vec{\mathcal{E}}(t), \quad (5)$$

$\vec{\mu}(R, r)$ being the molecular dipole moment and $\vec{\mathcal{E}}(t)$ the electric field vector of the linearly polarized laser. In the presence of an electric field, the dipole moment can be expressed as [17]

$$\vec{\mu} = \vec{\mu}_0 + \frac{1}{2}\alpha\vec{\mathcal{E}} + \frac{1}{6}\beta\vec{\mathcal{E}}^2 + \frac{1}{24}\gamma\vec{\mathcal{E}}^3 + \dots, \quad (6)$$

where $\mu_0(R, r)$ is the permanent dipole moment, α is the polarizability tensor, and β and γ are the first and second hyperpolarizability tensors. From this series, we will retain only $\mu_0(R, r)$ and the components of the polarizability tensor α parallel $\alpha_{\parallel}(R, r)$ and perpendicular $\alpha_{\perp}(R, r)$ to the molecular axis. (Their values for the HCN molecule are taken from Refs. [4], [18], and [19]; see Table I.) We can therefore write

$$\begin{aligned} \hat{H}_L &= -\mu_0(R, r)\mathcal{E}(t)\cos\theta \\ &\quad - \frac{\mathcal{E}^2(t)}{2} [\alpha_{\parallel}(R, r)\cos^2\theta + \alpha_{\perp}(R, r)\sin^2\theta]. \end{aligned} \quad (7)$$

The molecular potential $V(R, r)$ used in the present study was obtained from Bowman *et al.* [20].

The projection M_J of the total angular momentum J on the laser polarization axis a good quantum number since the molecule-laser interaction is independent of φ . Furthermore, the use of a linearly polarized laser implies the selection rule

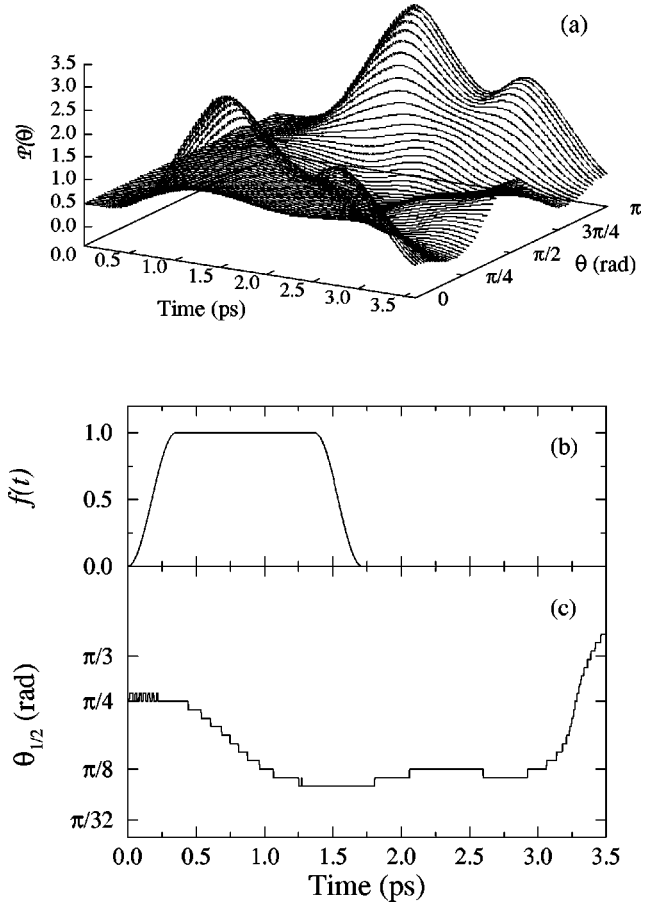


FIG. 2. (a) 3D plot of an angular distribution $\mathcal{P}(\theta)$, (b) field envelope $f(t)$, given by Eq. (11), and (c) half angle $\theta_{1/2}$ as a function of time. The angles θ and $\theta_{1/2}$ are expressed in radians. (An initial $J=0$ state in a $\omega=1075.0 \text{ cm}^{-1}$ laser field at $\mathcal{I} = 10^{13} \text{ W/cm}^2$ is used as an example.)

$\Delta M_J = 0$, so M_J will remain constant. The initial wave function is taken as the ground vibrational $v=0$ and rotational $J=M_J=0$ state. The propagation of the wave function $\psi(R, r, \theta, \varphi; t)$, the solution of the TDSE with the Hamiltonian (1), is carried out using a split-operator technique [21,22] in conjunction with the scheme developed by Dateo and Metiu [23,13] for the angle variables.

B. Alignment measurement

The alignment dynamics is observed through the time-dependent angular distribution given as a density of probability integrated over R and r :

$$\mathcal{P}(\theta; t) = \int_{r_{\min}}^{r_{\max}} \int_{R_{\min}}^{R_{\max}} |\psi(R, r, \theta; t)|^2 R^2 dR r^2 dr. \quad (8)$$

To have a quantitative measure of the alignment of the molecule, we use the half angle $\theta_{1/2}$, defined by [24]

$$\int_0^{\theta_{1/2}} \mathcal{P}(\theta; t) d\theta = \frac{1}{2} \int_0^{\pi/2} \mathcal{P}(\theta; t) d\theta. \quad (9)$$

Figure 2 shows the correspondence between an angular distribution $\mathcal{P}(\theta; t)$ and the half angle $\theta_{1/2}$ calculated from

Eq. (9) for the example of an initial $J=0$ state in a CO_2 laser field at 10^{13} W/cm^2 . At $t=0$ ps, we have an isotropic distribution in θ , giving a half-angle value of $\pi/4$. As we start to see alignment towards $\theta=0$, from $t=0.5$ ps to 1.5 ps, the $\theta_{1/2}$ value goes down to below $\pi/8$. Conversely, the angular distribution centered on $\pi/2$ observed at the end is translated into a high value for the half angle. (The steps observed in the half-angle curve are due to the discretization of the angular variable θ .) Note that this method of measuring the alignment is biased towards $\theta=0$ and $\pi/2$. A peak centered on $\pi/4$ would result in a value of $\theta_{1/2}$ of $\pi/4$, the same as was noted above for an isotropic distribution. Also, all probability distributions in this paper are symmetric about $\pi/2$, eliminating the need of doing the same exercise from $\theta = \pi/2$ to π . As indicated previously, initially the molecule is in rotational state $J=M_J=0$, corresponding to the isotropic case for which $\theta_{1/2}=\pi/4$.

C. Description of the laser pulses

The laser pulses used in our calculations are defined by

$$\mathcal{E}(t)=f(t)\mathcal{E}_0\cos(\omega t), \quad (10)$$

where the field envelope is given by

$$f(t)=\begin{cases} \sin^2\left[\frac{t}{t_i}\frac{\pi}{2}\right] & \text{if } 0<t<t_i \\ 1 & \text{if } t_i\leq t<t_p-t_i \\ \sin^2\left[\frac{t-t_p}{t_i}\frac{\pi}{2}\right] & \text{if } t_p-t_i\leq t<t_p \\ 0 & \text{elsewhere,} \end{cases} \quad (11)$$

with $t_p=1.7$ ps the total pulse duration and $t_i=0.35$ ps the turn-on/off time; see Fig. 2(b). Such a slow rise and fall of the laser pulse is adiabatic with respect to vibrational but not rotational levels. The maximum field amplitude \mathcal{E}_0 corresponds to a peak intensity of $\mathcal{I}=10^{13} \text{ W/cm}^2$. From the tunneling model of ionization, which is valid at low frequencies, e.g., IR, the intensity threshold for ionization is [25,26]

$$\mathcal{I}_i(\text{W/cm}^2)=4\times 10^9[V_{\text{ion}}(\text{eV})]^4Z^{-2}, \quad (12)$$

where V_{ion} is the ionization potential and Z is the total residual charge. For the first ionization threshold ($Z=1$) of HCN with $V_{\text{ion}}=13.60$ eV [27] (similar to that of H), we readily obtain

$$\mathcal{I}_i=1.4\times 10^{14} \text{ W/cm}^2. \quad (13)$$

Thus, for HCN, laser intensities below 10^{14} W/cm^2 can be used for nonlinear optical effects without any laser damage through ionization in the IR region. These intensities constitute a lower threshold for the nonlinear effects with respect to vibrations. Actually, an estimate for the Rabi frequencies corresponding either to the permanent-dipole-moment interaction

$$\omega_R^{(\mu_0)}=\hbar^{-1}\mathcal{E}_0\langle\chi_1|\mu_0|\chi_0\rangle \quad (14)$$

or to the polarizability interaction

$$\omega_R^{(\alpha)}=\hbar^{-1}\mathcal{E}_0^2\langle\chi_1|\alpha|\chi_0\rangle \quad (15)$$

leads to a result not exceeding 100 cm^{-1} , less than the vibrational energy separations. However, these Rabi frequencies are much larger than the rotational energy separations, at least up to $J=30$.

The laser frequencies, taken in the infrared spectrum, are either the $\omega=1075.0 \text{ cm}^{-1}$ line of a CO_2 laser ($\lambda=9.3 \mu\text{m}$) or directly in resonance with the first and second vibrational excitations of HCN, 2095.4 cm^{-1} and 3352.8 cm^{-1} , basically corresponding to $\text{C}\equiv\text{N}$ and $\text{C}-\text{H}$ bond excitations, respectively. In the cases where we will leave only one bond free to vibrate, the excitation frequencies become 3211.3 cm^{-1} for $\text{C}-\text{H}$ and 2323.7 cm^{-1} for $\text{C}\equiv\text{N}$ due to the neglect of the interbond interaction. Such IR frequencies at intensities $\mathcal{I}\leq 10^{13} \text{ W/cm}^2$ are currently available with modern laser technology [28].

D. Laser-driven rigid-rotor approximation

A first simplification of this three-degree-of-freedom model, which is still relevant for a dynamical approach of the alignment, is to freeze the stretching degree of freedom and consider a laser-driven rigid rotor. In order to have an intuitive insight for the interpretation of our results, we proceed now to the derivation of the classical equation of motion of a rigid rotor interacting with an electromagnetic field through the combined effect of a dipole moment and a polarizability. We follow closely the derivation given by Landau and Lifshitz [29]. The Lagrangian is written as

$$L=\frac{I}{2}[\dot{\theta}^2+\sin^2\theta\dot{\varphi}^2]+\mu_0\mathcal{E}_0\cos\theta\cos\omega t +\frac{1}{2}\mathcal{E}_0^2[\alpha_{\parallel}\cos^2\theta+\alpha_{\perp}\sin^2\theta]\cos^2\omega t. \quad (16)$$

Lagrange equations involving θ and φ can be recast into a unique equation of motion for θ :

$$I\ddot{\theta}=\frac{M^2}{I}\frac{\cos\theta}{\sin^3\theta}-\frac{\alpha\mathcal{E}_0^2}{4}\sin 2\theta-\mu_0\mathcal{E}_0\sin\theta\cos\omega t -\frac{\alpha\mathcal{E}_0^2}{4}\sin 2\theta\cos 2\omega t, \quad (17)$$

where

$$\alpha=\alpha_{\parallel}-\alpha_{\perp} \quad (18)$$

and M is a constant of motion given by

$$M=I\sin^2\theta\dot{\varphi}. \quad (19)$$

As usual, the dots and double dots indicate first- and second-order derivatives with respect to time. If HCN is to be described as a rigid rotor, the most common situation would be the one that is termed *rotationally off resonance* in the sense that

$$\omega\gg\frac{d\theta}{dt}, \quad (20)$$

as the laser frequency ω (see Sec. II C) is expected to be much larger than the rotational frequency. Within the frame of this high-frequency assumption, the right-hand side of Eq. (17) gives rise to two classes of terms: time-independent and rapidly oscillating time-dependent ones. It is worthwhile noting that the radiative interaction is already present in the time-independent term, but only through the polarizability α . $\theta(t)$ follows a smoothly varying trajectory, perturbed by small-amplitude oscillations $\xi(t)$ of frequency ω , which are approximately solutions of the time-dependent part of Eq. (17):

$$I\ddot{\xi} = -\mu_0\mathcal{E}_0\sin\theta\cos\omega t - \frac{\alpha\mathcal{E}_0^2}{4}\sin 2\theta\cos 2\omega t. \quad (21)$$

From Eq. (21) one can calculate the average kinetic energy of the oscillatory motion by integrating once and squaring:

$$\frac{I}{2}\overline{\dot{\xi}^2} = \frac{\mu_0^2\mathcal{E}_0^2}{4I\omega^2}\sin^2\theta + \frac{\alpha^2\mathcal{E}_0^4}{256I\omega^2}\sin^2 2\theta \quad (22)$$

(the bar over $\dot{\xi}^2$ meaning an average over one optical cycle). An equation of motion for θ is then obtained in terms of an effective force field derived from the sum of a time-independent potential $V(\theta)$ and the time-averaged kinetic energy

$$I\ddot{\theta} = -\frac{dV_{\text{eff}}}{d\theta}, \quad (23)$$

where

$$V_{\text{eff}} = V(\theta) + \frac{I}{2}\overline{\dot{\xi}^2}, \quad (24)$$

with

$$-\frac{dV}{d\theta} = \frac{M^2\cos\theta}{I\sin^3\theta} - \frac{\alpha\mathcal{E}_0^2}{4}\sin 2\theta. \quad (25)$$

One finally gets

$$\ddot{\theta} = \frac{M^2\cos\theta}{I^2\sin^3\theta} - \left[\frac{\mu_0^2\mathcal{E}_0^2}{4I^2\omega^2} + \frac{\alpha\mathcal{E}_0^2}{4I} \right] \sin 2\theta - \frac{\alpha^2\mathcal{E}_0^4}{128I^2\omega^2}\sin 4\theta. \quad (26)$$

A further simplification consists in neglecting the higher-order correction term proportional to \mathcal{E}_0^4/ω^2 , taking $M=0$ [which means that φ is time independent; see Eq. (19)], and making the substitution $\Theta = 2\theta$, to end up with

$$\ddot{\Theta} + \Omega^2\sin\Theta = 0, \quad (27)$$

where the frequency Ω is

$$\Omega = \frac{1}{\sqrt{I}} \left(\frac{1}{2} \frac{\mu_0^2\mathcal{E}_0^2}{I\omega^2} + \frac{1}{2} \alpha\mathcal{E}_0^2 \right)^{1/2}. \quad (28)$$

Equation (27) can be solved either exactly or approximately for $\Theta \approx 0$ by merely assuming that $\sin\Theta \approx \Theta$, which leads to

a harmonic oscillation for Θ . A dynamical alignment time for Θ (i.e., for θ) can then be defined by referring to the oscillation period τ proportional to Ω^{-1} [30]. We also define the concept of a dynamical alignment rate proportional to the inverse of the alignment time, i.e., proportional to Ω . A closer inspection of the above derivation leads to the following considerations in the high-frequency off-resonance regime.

(i) The permanent dipole moment part of the radiative interaction $\mu_0\mathcal{E}_0\cos\omega t$ oscillates very rapidly with the field and its mean value averages to zero over the optical cycle. However, the second-order field-induced dipole moment $\mu_0^2\mathcal{E}_0^2\cos^2\omega t$ and the polarizability $\alpha\mathcal{E}_0^2\cos^2\omega t$ average to $\mu_0^2\mathcal{E}_0^2/2$ (with a renormalization factor $I\omega^2$, resulting from virtual excitations of energy $I\omega^2$ in a quantum picture) and $\alpha\mathcal{E}_0^2/2$, respectively, over the optical cycle and thus contribute on an equal footing to the θ motion and to its frequency Ω .

(ii) The ratio of the second-order dipole moment to the polarizability contribution in Ω is independent of the field amplitude and, for the parameters of the model under consideration, is (see Table I for values)

$$\left(\frac{\mu_0^2\mathcal{E}_0^2}{2I\omega^2} \right) \left(\frac{\alpha\mathcal{E}_0^2}{2} \right)^{-1} \approx 2.1 \times 10^{-6} [\omega(\text{a.u.})]^{-2}. \quad (29)$$

Polarizability is thus the leading contribution when the field frequency exceeds 1.4×10^{-3} a.u. (315 cm^{-1}), whatever the intensity.

(iii) The ratio of the neglected term in Eq. (26) to the leading polarizability contribution is

$$\left(\frac{\alpha^2\mathcal{E}_0^4}{128I\omega^2} \right) \left(\frac{\alpha\mathcal{E}_0^2}{4} \right)^{-1} \approx 3.5 \times 10^{-6} \left[\frac{\mathcal{E}_0(\text{a.u.})}{\omega(\text{a.u.})} \right]^2, \quad (30)$$

which is several orders of magnitude smaller than 1 for the field frequencies ($\omega \geq 1075 \text{ cm}^{-1} = 4.9 \times 10^{-3}$ a.u.) and intensities ($\mathcal{I} = 10^{13} \text{ W/cm}^2$, corresponding to $\mathcal{E}_0 = 1.7 \times 10^{-2}$ a.u.) considered in this work.

Completely different dynamics would result in the low-frequency resonant regime [i.e., for $\omega \sim d\theta/dt$, or equivalently, $\theta(t) \approx \omega t$]. The equation of motion in the frame of the rotating-wave approximation [obtained by neglecting terms in $\theta + \omega t$ and 2θ , rapidly oscillating as compared to $\theta - \omega t$, in Eq. (17)] is, taking $M=0$,

$$\ddot{\theta} = -\frac{\mu_0\mathcal{E}_0}{2I}\sin(\theta - \omega t) - \frac{\alpha\mathcal{E}_0^2}{8I}\sin 2(\theta - \omega t), \quad (31)$$

which, by an appropriate change of variable $\Theta = \theta - \omega t$, can be recast into

$$\ddot{\Theta} + \frac{\mu_0\mathcal{E}_0}{2I}\sin\Theta + \frac{\alpha\mathcal{E}_0^2}{8I}\sin 2\Theta = 0, \quad (32)$$

which, for small values of Θ (i.e., with $\sin 2\Theta \sim 2\sin\Theta$), is the resonant counterpart of Eq. (27):

$$\ddot{\Theta} + \tilde{\Omega}^2\sin\Theta = 0, \quad (33)$$

where the corresponding frequency is now

$$\tilde{\Omega} = \left(\frac{\mu_0 \mathcal{E}_0}{2I} + \frac{\alpha \mathcal{E}_0^2}{4I} \right)^{1/2}. \quad (34)$$

The ratio of the contribution of the permanent dipole moment to that of the polarizability in $\tilde{\Omega}$ is field-amplitude dependent with

$$\left(\frac{\mu_0 \mathcal{E}_0}{2I} \right) \left(\frac{\alpha \mathcal{E}_0^2}{4I} \right)^{-1} \approx 2.7 \times 10^{-1} [\mathcal{E}_0 (\text{a.u.})]^{-1}. \quad (35)$$

μ_0 remains the leading term at least for intensities not exceeding $2.6 \times 10^{15} \text{ W/cm}^2$ (note that $\mathcal{E}_0 = 1 \text{ a.u.}$ corresponds to an intensity $\mathcal{I} = 3.5 \times 10^{16} \text{ W/cm}^2$) in the rotationally resonant case.

In summary, from Eq. (29), we expect that for IR frequencies well above the rotational frequency, as with a CO_2 laser, one expects the main molecule-field interaction to be mediated by the polarizability of the molecule if internal vibrational excitations can be neglected.

III. RESULTS

Alignment dynamics is studied by referring to two observables: the behavior of the half angle $\theta_{1/2}$ as a function of time and the rovibrational distributions of the excited species at the end of the laser pulse. The results are presented for three different laser frequencies by comparing in each case models of increasing complexity with respect to the number of degrees of freedom: from the oversimplified rigid rotor involving a unique angular variable θ positioning the linear HCN molecule (without any internal degree of freedom) with respect to the field polarization vector, which we call the one-dimensional (1D) model, to HCN with an additional internal stretching motion (either C—H or C \equiv N), which we call the 2D model, and finally to HCN still considered linear but described by its two internal stretching motions, the 3D model. This is, to the best of our knowledge, the first attempt, in the intense-field alignment context, of a wavepacket propagation under a relatively long picosecond pulse on a three-dimensional grid (two radial and one angular variables) to study the influence of internal dynamics on the alignment process.

A. Half-angle dynamics: Characteristic features

The results of the half-angle dynamics are presented for the three models under consideration, i.e., the 1D rigid rotor, the two versions of 2D models (C—H or C \equiv N bond free to vibrate), and the full 3D model for HCN. The displayed data allow for a separate analysis of the role played in alignment by the permanent dipole μ_0 or the polarizability α when taken alone and when they are combined. To facilitate the lecture of the graphs, we emphasize some salient features of the high-frequency regime [as defined by Eq. (20)] that are characteristic of all the results to be discussed (see Fig. 4, for example).

(i) *During the pulse* ($t \leq 1.7 \text{ ps}$). A more or less sharp decrease of the half angle $\theta_{1/2}$ follows the switching on of the pulse [Fig. 2(b)] after a time delay corresponding roughly

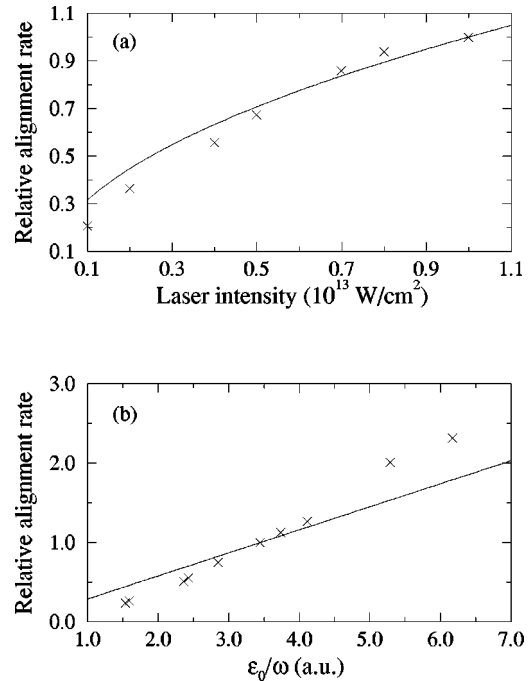


FIG. 3. Relative alignment rate for the rigid rotor calculated numerically (\times) and expected from Eq. (28) (solid line) for (a) α alone at frequency $\omega = 1075.0 \text{ cm}^{-1}$ (intensity $\mathcal{I} = 10^{13} \text{ W/cm}^2$ used as a reference point) and (b) μ_0 alone (intensity $\mathcal{I} = 10^{13} \text{ W/cm}^2$ and frequency $\omega = 1075.0 \text{ cm}^{-1}$, giving $\mathcal{E}_0/\omega = 3.446 \text{ a.u.}$, used as a reference point).

to 0.2 ps. The slope of $\theta_{1/2}$ itself is indicative of a dynamical alignment rate and is correlated to the alignment time as defined in the rigid-rotor model. More precisely, as seen from Eq. (28), when α is considered alone, an increasing intensity \mathcal{E}_0^2 (\mathcal{I}) results in a shorter alignment time τ inversely proportional to the square root of the laser intensity \mathcal{I} ($\tau \propto 1/\mathcal{E}_0$). On the other hand, μ_0 taken alone leads to an alignment time proportional to ω/\mathcal{E}_0 (or $\omega/\mathcal{I}^{1/2}$). Figure 3 compares, within the rigid-rotor model, the dynamical alignment rates (28) with the relative slope of $\theta_{1/2}(t)$ for short times. This comparison is done both for α taken alone [for different intensities, Fig. 3(a)] and for μ_0 taken alone [for different ratios \mathcal{E}_0/ω , Fig. 3(b)]. Fairly good agreement is obtained, opening up the possibility of a quantitative measure of the dynamical alignment rate in terms of the slope of the half angle at short times, in all cases to be compared. From the overall behavior, marked differences are observed for μ_0 and α taken separately, α leading to strong alignment within 0.6 ps ($\theta_{1/2}$ decreasing to such values as $\pi/32$) followed by oscillations, whereas μ_0 affects the alignment dynamics by regularly decreasing $\theta_{1/2}$ during the whole pulse duration but to a lesser extent. The combined action of μ_0 and α follows rather closely the dynamics induced by α alone, showing the leading role of the polarizability in agreement with Eq. (29). At the end of the pulse ($t = 1.7 \text{ ps}$) the molecule shows an alignment with the field to an extent of $\theta_{1/2} \approx \pi/16$.

(ii) *Postpulse dynamics* ($t > 1.7 \text{ ps}$). Different excitation regimes and models lead to more marked deviations with a wide range of oscillation amplitudes in $\theta_{1/2}(t)$. Large amplitudes are the signatures of the propensity of the molecule to

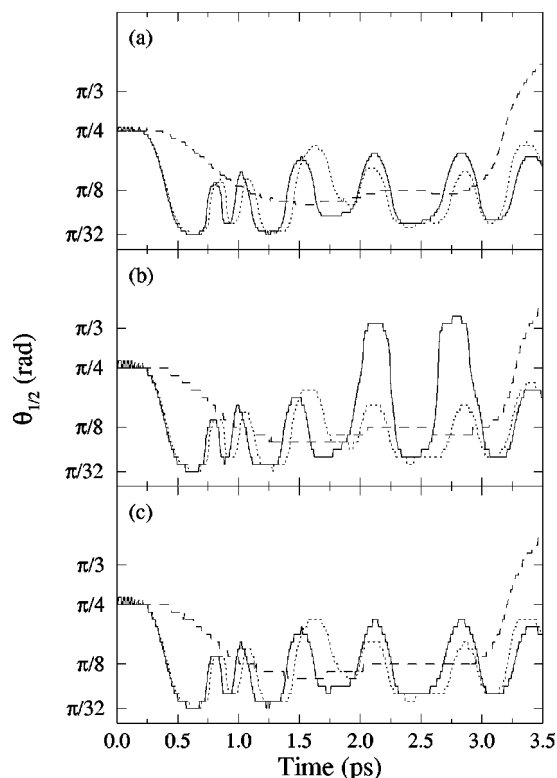


FIG. 4. Half-angle values $\theta_{1/2}$ for a laser frequency of $\omega = 1075.0 \text{ cm}^{-1}$ and intensity of $\mathcal{I} = 10^{13} \text{ W/cm}^2$ for (a) the rigid rotor, (b) the 2D model with the C—H bond free to vibrate, and (c) the 2D model with the C \equiv N bond free to vibrate, using in the laser-molecule interaction only the permanent dipole moment μ_0 (dashed line), only the polarizability α (dotted line), or both (solid line), as a function of time.

lose its alignment characteristics due to dephasing and rephasing of the coherently excited rotational levels. Some interpretative schemes can be derived by considering the rovibrational populations at the end of the pulse. This information is, in principle, enough to obtain the postpulse features of the dynamics by avoiding prohibitively time-consuming wave-packet propagations. Such a comparison in a 2D model, between a full wave-packet propagation and a simplified calculation based on a spherical harmonics expansion of the wave packet at the end of the pulse, propagated (in the absence of the laser) using the appropriate phases, leads to excellent agreement in the half-angle dynamics. The observed beats can be interpreted in terms of coherent superpositions of rotational states from the initial $J=0$ state considered here. For example, in the 2D CH model [Fig. 4(b)] $J=0$ (30%), $J=2$ (48%), and $J=6$ (19%) are the most populated rotational states at the end of the pulse [see Fig. 5(b)]. Their energy separations $\Delta E_{J,J'}$, equal to $\Delta E_{6,2} = 36B_0$ and $\Delta E_{6,0} = 42B_0$, result in oscillations periods of 0.63 ps and 0.54 ps, respectively, which is roughly the main oscillation observed in the figure. [$\Delta E_{2,0} = 6B_0$ gives an oscillation period of 3.8 ps, which is too long to appear in Fig. 4(b).]

We proceed next to a detailed comparison between the different excitation regimes. The laser frequencies are chosen either off or on resonance with respect to vibrational fre-

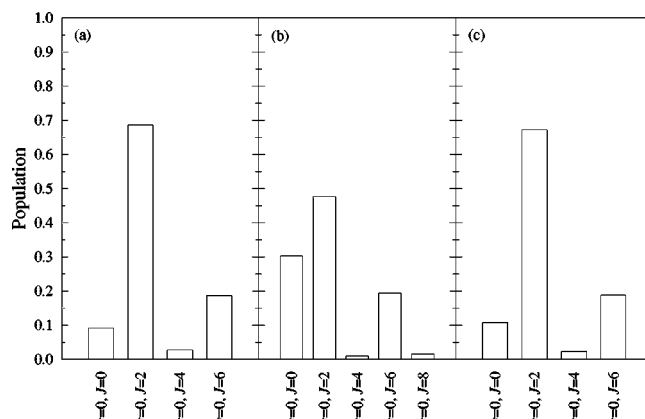


FIG. 5. Rovibrational population at the end of the pulse for a laser frequency of $\omega = 1075.0 \text{ cm}^{-1}$ and intensity of $\mathcal{I} = 10^{13} \text{ W/cm}^2$ for (a) the rigid rotor, (b) the 2D model with the C—H bond free to vibrate, and (c) the 2D model with the C \equiv N bond free to vibrate, using in the laser-molecule interaction both the permanent dipole moment μ_0 and the polarizability α . (Only levels with a population greater than 1% are given.)

quencies, but in all cases remaining rotationally nonresonant [as given by Eq. (20)].

B. Off-resonance excitation ($\omega = 1075 \text{ cm}^{-1}$)

Figures 4 and 5 summarize the results for the 1D rigid rotor and for the two versions of the 2D model, i.e., either the CH or CN bond is free to vibrate with the other frozen. The time-dependent behavior of the half angle $\theta_{1/2}$ when the pulse is on [see Fig. 2(b)] seems rather similar for all models, in particular when α or μ_0 is treated separately. This is not surprising since HCN restricted to collinear geometry and excited in an off-resonance way avoiding vibrational energy deposit in the CH or CN bonds is actually expected to behave as a rigid rotor. The dynamical alignment rates, as derived from the slopes of $\theta_{1/2}(t)$ for short times, are very close to each other. Finally, the 3D model, for the dipole-interaction case, was found to give rise to comparable alignment dynamics and therefore is not shown. We can see that α predominates, as expected from Eqs. (28) and (29), the ratio $\mu_0^2/\alpha I \omega^2$ being equal to 8.8×10^{-2} at $\mathcal{I} = 10^{13} \text{ W/cm}^2$ and $\omega = 1075.0 \text{ cm}^{-1}$.

The rotational distribution at the end of the pulse (Fig. 5), responsible for the subsequent field-free evolution, shows three features that deserve interest.

(i) There is a parity conservation law for the rotational excitation (starting from $J=0$, only even- J levels are populated). Each photon absorption-emission process being accompanied by a change of but one quantum number J , the even parity is the signature of the absence of direct rotational transitions. The populations of higher J levels are reached, in the case of off-resonance laser excitation, via virtual photon absorption-emission processes. As is clear from the rigid-rotor model [Eq. (26)], second-order radiative couplings are responsible for the transitions, leading thus to $\Delta J = 0, \pm 2$ selection rules.

(ii) In both models, at least half of the population is transferred from the initial $J=0$ to $J=2$ (69% for the rigid rotor and 48% and 67% for the 2D models with CH and CN re-

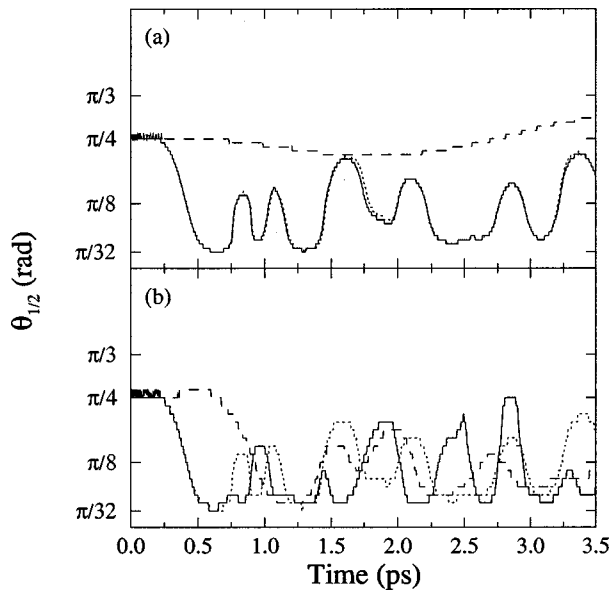


FIG. 6. Half-angle values $\theta_{1/2}$ for a laser frequency of $\omega = 3211.3 \text{ cm}^{-1}$ (on resonance with the C—H bond) and intensity of $\mathcal{I} = 10^{13} \text{ W/cm}^2$ for (a) the rigid rotor and (b) the 2D model with the CH bond free to vibrate, using only μ_0 (dashed line), only α (dotted line), or both (solid line).

spectively). The rigid-rotor model gives a rotational distribution closer to that of the 2D model with the frozen CH bond.

(iii) The differences in phase between the populated J levels are responsible for the beats observed in $\theta_{1/2}$ in the field-free region, as explained in Sec. III A. The molecule is periodically realigned, but some oscillation amplitudes in $\theta_{1/2}$ are larger in the 2D model with the frozen CN bond.

C. Resonant excitation

The results are displayed in Figs. 6 and 7 for the vibrationally resonant excitation of the CH bond and in Figs. 8 and 9 for CN, with the other bond frozen (2D model). Figures 10 and 11 illustrate results for calculations of the TDSE

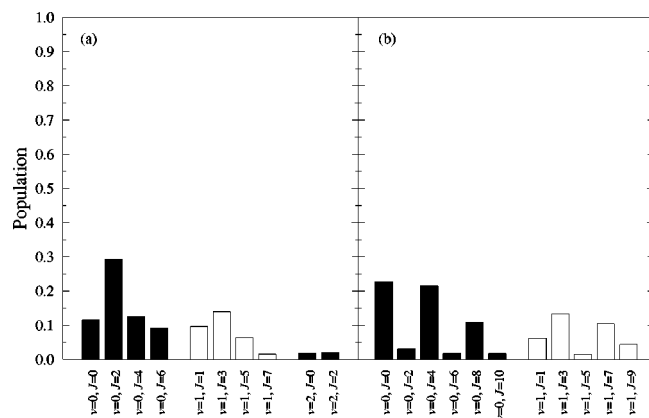


FIG. 7. Rovibrational population at the end of the pulse for a laser frequency of $\omega = 3211.3 \text{ cm}^{-1}$ (on resonance with the C—H bond) and intensity of $\mathcal{I} = 10^{13} \text{ W/cm}^2$ for the 2D model with the C—H bond free to vibrate, using in the laser-molecule interaction (a) only the permanent dipole moment μ_0 and (b) both μ_0 and the polarizability α . (Only levels with a population greater than 1% are given.)

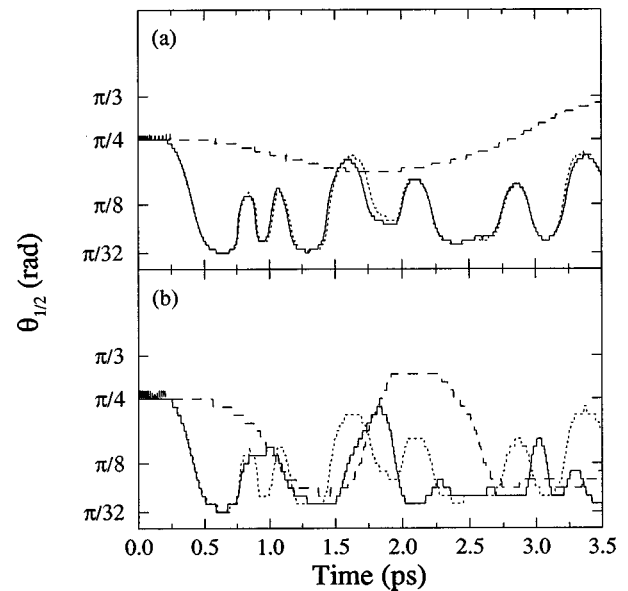


FIG. 8. Half-angle values $\theta_{1/2}$ for a laser frequency of $\omega = 2323.7 \text{ cm}^{-1}$ (on resonance with the C \equiv N bond) and intensity of $\mathcal{I} = 10^{13} \text{ W/cm}^2$ for (a) the rigid rotor and (b) the 2D model with the CN bond free to vibrate, using only μ_0 (dashed line), only α (dotted line), or both (solid line).

with the full dynamics included, i.e., both bonds are free (3D model). The analysis is conducted along the same lines as previously.

During the pulse, the alignment dynamics of the rigid rotor [Figs. 6(a) and 8(a)] under the action of the dipole moment μ_0 is markedly different from the other models (2D and 3D) [Figs. 6(b), 8(b), and 10]. The role of μ_0 in the rigid rotor is nearly washed out due to the high frequency [Eq. (26)], especially in the case of $\omega = 3211.3 \text{ cm}^{-1}$ corresponding to the CH resonant excitation. On the contrary, this role is enhanced in the 2D models as μ_0 is responsible for the stretching-mode motions that are resonantly excited. The coupling responsible for $\Delta v = 1$ transitions from vibrational state χ_0 to χ_1 is

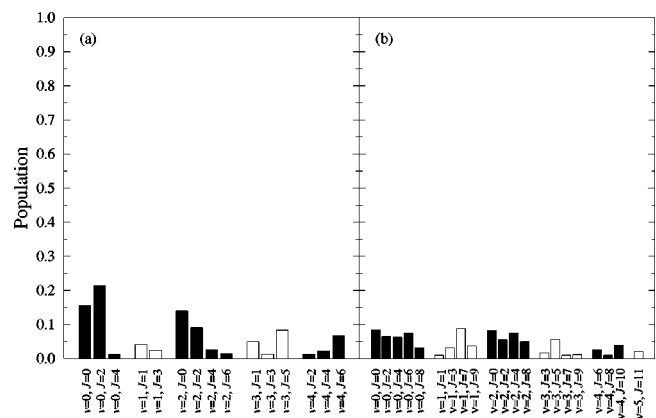


FIG. 9. Rovibrational population at the end of the pulse for a laser frequency of $\omega = 2323.7 \text{ cm}^{-1}$ (on resonance with the C \equiv N bond) and intensity of $\mathcal{I} = 10^{13} \text{ W/cm}^2$ for the 2D model with the C \equiv N bond free to vibrate, using in the laser-molecule interaction (a) only the permanent dipole moment μ_0 and (b) both μ_0 and the polarizability α . (Only levels with a population greater than 1% are given.)

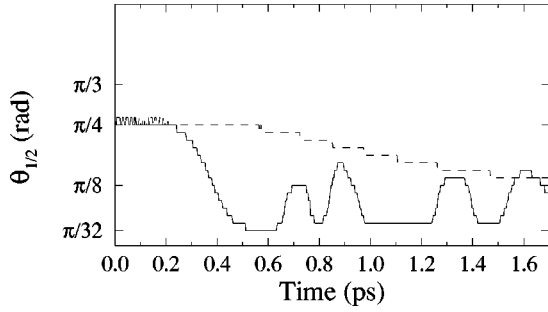


FIG. 10. Half-angle values $\theta_{1/2}$ for a laser frequency of $\omega = 2095.4 \text{ cm}^{-1}$ (on resonance with the $\text{C}\equiv\text{N}$ bond) and intensity of $\mathcal{I} = 10^{13} \text{ W/cm}^2$ for the 3D model, using only μ_0 (dashed line) or both μ_0 and α (solid line).

$$\langle \chi_1(R) | \mu_0(R) | \chi_0(R) \rangle = 2.53 \times 10^{-2} \text{ a.u.} \quad (36)$$

for the CH bond and

$$\langle \chi_1(r) | \mu_0(r) | \chi_0(r) \rangle = -1.14 \times 10^{-2} \text{ a.u.} \quad (37)$$

for the CN bond, in the 2D models. The factor of 2 between these couplings can explain the difference of slopes observed for $\theta_{1/2}$ in CH [Fig. 6(b)] and CN [Fig. 8(b)] when μ_0 is considered alone.

At the end of the pulse, in the case of the CH excitation (Fig. 7), the population that ends up in the $v=1$ excited vibrational state ($\approx 35\%$) is composed of odd- J rotational levels, while the $v=0$ level shows only even J 's up to 10. The role of the dipole moment interaction, when considered alone, is examined in Fig. 7(a). The leading ($v=0, J=2$) population is probably due to the biphotonic $\mu_0^2 \mathcal{E}^2$ interaction. The polarizability acts by increasing the rotational excitation. Figure 7(b) shows the population resulting from the combined effect of μ_0 and α . In the case of the CN excitation (Fig. 9) significant population is seen up to the $v=4$ level ($\approx 10\%$) together with higher rotational level populations reaching 4% in $J=10$ (in the $v=4$ state) and 2% in $J=11$ (in the $v=5$ state) when both μ_0 and α are present. This is the result of higher harmonicity and larger polariz-

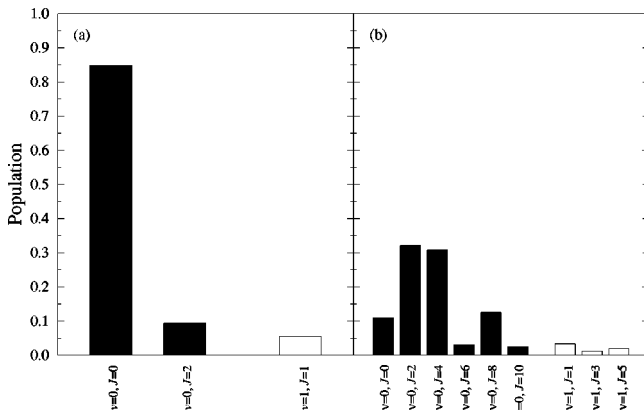


FIG. 11. Rovibrational population at the end of the pulse for a laser frequency of $\omega = 2095.4 \text{ cm}^{-1}$ (on resonance with the $\text{C}\equiv\text{N}$ bond) and intensity of $\mathcal{I} = 10^{13} \text{ W/cm}^2$ for the 3D model, using in the laser-molecule interaction (a) only the permanent dipole moment μ_0 and (b) both μ_0 and the polarizability α . (Only levels with a population greater than 1% are given.)

ability of the CN bond. High J 's are more efficiently populated by pumping the molecule through vibrational resonant excitation as in the case of CN (population of higher J 's is a necessary condition for obtaining greater alignment).

The different parity rules for J that are observed, as compared to the off-resonance case, are related to the occurrence of a vibrational excitation. The resonant character of the laser allows a direct transition with $\Delta v = 1$ and $\Delta J = 1$ by absorbing a single photon through the first-order dipole interaction $\mu_0 \mathcal{E}_0$. More than one photon can be absorbed through second-order radiative interactions in $\alpha \mathcal{E}_0^2$ or $\mu_0^2 \mathcal{E}_0^2$ leading to $\Delta v = 0$ and $\Delta J = 0, 2$.

We note that a general state created by the laser field is a superposition, in the resonant case, of different v 's and J 's, i.e.,

$$\psi(R, r, \theta; t) = \sum_{v, J} c_{v, J}(t) \chi_v(R, r) Y_J(\theta). \quad (38)$$

However, due to the orthogonality of the vibrational functions $\chi_v(R, r)$, the time-dependent angular distribution $\mathcal{P}(\theta; t)$ [Eq. (8)], after integrating out the vibrational coordinates R and r ,

$$\mathcal{P}(\theta; t) = \sum_v \sum_{J, J'} c_{v, J}^*(t) c_{v, J'}(t) Y_J^*(\theta) Y_{J'}(\theta), \quad (39)$$

shows no interference between different parity angular partial waves since J and J' have the same parity for a given v . Such angular distributions therefore show no asymmetry, i.e., no symmetry breaking with respect to $\pi/2$, hence no orientation. Low-frequency rotational quantum beats ($\tau \approx 0.6 \text{ ps}$; see Figs. 4, 6, and 8) remain between rotational states of same-parity quantum states J and J' in the same vibrational level v .

The present result shows that single laser excitations will produce alignment only [$\mathcal{P}(\theta) = \mathcal{P}(\pi - \theta)$], but *no* orientation [$\mathcal{P}(\theta) \neq \mathcal{P}(\pi - \theta)$], even though different-parity optical processes, even for α and odd for μ_0 , are occurring simultaneously. As emphasized earlier, parity or symmetry breaking and hence orientation requires two lasers, one of frequency ω and the other of frequency 2ω . This has been shown previously to lead to separation of photodissociation products [8,9]. In the case of bound-state excitation as studied here for HCN, resonant excitation of CH or CN bonds via the dipole term at frequencies $\omega = \omega_{\text{CH}}$ or ω_{CN} must be accompanied by a second laser of frequency $\frac{1}{2}(\omega_{\text{CH}}$ or $\omega_{\text{CN}})$ in order to produce concomitant resonant excitation of these bonds via the polarizability interaction. In summary, in the present single-laser excitation, only alignment but no orientation can be achieved in the presence of simultaneous dipole- and polarizability-field interactions.

The full dynamics, in the 3D model, is studied under a laser excitation of frequency $\omega = 2095.4 \text{ cm}^{-1}$, which is resonant with the CN local stretch. The behavior of the half angle (Fig. 10) remains within the general trend of previous calculations showing a nice alignment of the molecule during the laser pulse. The oscillations between $\pi/32$ and $\pi/8$ seem even of smaller amplitude than those observed in the 2D models. The population distributions given in Fig. 11 show, in contrast to the case of the resonantly excited CN of

the 2D calculation (Fig. 9), only weak vibrational excitation (less than 10%, whether only μ_0 or both μ_0 and α are introduced). This corroborates the fact that no infrared absorption is observed experimentally when exciting the symmetric normal stretch mode at $\omega = 2096.7 \text{ cm}^{-1}$ [31]. A simple analysis of the vibrational dipole matrix element provides an interpretation. A first-order expansion leads to

$$\begin{aligned} \langle \chi_1 | \mu_0(R, r) | \chi_0 \rangle &\approx \frac{\partial \mu_0}{\partial R} \langle \chi_1 | R - R_0 | \chi_0 \rangle \\ &+ \frac{\partial \mu_0}{\partial r} \langle \chi_1 | r - r_0 | \chi_0 \rangle. \end{aligned} \quad (40)$$

The matrix elements of $R - R_0$ and $r - r_0$ are both negative, whereas the derivatives of μ_0 are of opposite sign and nearly identical in absolute value, as can be seen from Table I. This is at the origin of a near cancellation of the right-hand side of Eq. (40) resulting in a suppression of vibrational excitation. Actually, we have also proceeded to a numerical test of this interpretation by freezing the R dependence of the dipole moment, i.e., taking $\partial \mu_0 / \partial R = 0$. The aforementioned cancellation can no longer occur in Eq. (40) and, as expected, a richer vibrational spectrum extending beyond $v=1$ is obtained.

IV. CONCLUSION

Laser-induced alignment of a prototypical polyatomic molecule, HCN, was studied by numerical solution of the corresponding TDSE, which included internal excitations and dynamics. Both permanent dipole moments and polarizabilities were included in the full quantum dynamical calculation, which excluded only the bending of the molecule, a vibrational mode of lower frequency ($\approx 700 \text{ cm}^{-1}$ [20]) than the laser frequency used in the present calculations. Bending excitation would probably affect the alignment dynamics and this is to be examined in future work. A classical analytic model of the rigid rotor with the dipole- and polarizability-field interactions was used to interpret the alignment properties of HCN for laser frequencies nonresonant and resonant with the bond vibrations, CH and CN.

The calculated half angle $\theta_{1/2}$ [Eq. (9)] was used as a measure of alignment. It was found that for the three frequencies used, $\omega_{\text{CO}_2} = 1075.0 \text{ cm}^{-1}$, $\omega_{\text{CH}} = 3211.3 \text{ cm}^{-1}$, and $\omega_{\text{CN}} = 2323.7 \text{ cm}^{-1}$, at an intensity $\mathcal{I} = 10^{13} \text{ W/cm}^2$ (well below the ionization threshold), initial alignment occurred within 0.6 ps and this alignment is completely mediated by the polarizability α . Since the effective radiative interaction in this case is $\frac{1}{2} \alpha \mathcal{E}_0^2 \cos^2 \omega t$, this gives rise to resonant vibrational transitions at twice the frequency ω only, whereas the dipole interaction $\mu \mathcal{E}_0 \cos \omega t$ leads to resonant vibrational

transitions at frequency ω . For the three frequencies chosen, 2ω -frequency resonant transitions via α are therefore negligible. The predominance of the polarizability α as the major factor for the early alignment of HCN is nonresonant and creates even J 's. Dipole transitions occur in the resonant case, for both CH and CN bonds, thus adding odd rotational J states to the even- J states from the polarizability α to the total coherent state prepared by the laser excitation from an initial $J=0$ ground-state molecule. In the nonresonant case, only even J 's are excited. Thus, in the resonant case, complicated temporal quantum beats occur during and after the pulse due to a more complex coherent state when compared to the off-resonance case.

The resonant excitation case produces interesting coherent rotational states that contain both even- J partial waves from the nonresonant polarizability α and odd- J states from the resonant dipole term μ_0 . One would expect such states due to a mixture of different parities to break symmetry, hence producing anisotropies in the angular distribution of the molecule and leading perhaps to orientation as distinct from alignment. As shown in Sec. III C, in spite of the mixture of even and odd J 's, no orientation can be obtained in single-laser-frequency experiments due to the orthogonality of the internal vibrational states. A combination of two lasers, one at frequency ω (for resonant dipole transitions) and the other at frequency $\omega/2$ (for resonant polarizability transitions), is proposed to create such an orientation [8,9,32].

Finally, the usefulness of single-laser-frequency alignment is limited by the considerable temporal dephasing of an initially aligned molecule due to the coherent superposition of rotational states of different energies. A possible resolution of this limitation might be to use chirped pulses that will allow for more efficient rovibrational excitation [33] and perhaps could suppress quantum beats with an appropriate time-dependent phase $\phi(t)$. Another scenario being examined currently for the orientation case is to use the relative phase ϕ between the two lasers of frequencies ω and 2ω as a control parameter [34] to reduce the "noise," i.e., fluctuations in the orientation angle, which is determined by the relative laser intensities and transition moments, both dipole and polarizability in the total Hamiltonian (1).

ACKNOWLEDGMENTS

We wish to thank Dr. M. Raoult for his help with the calculation of the eigenstates of the HCN molecule. C.M.D. gratefully acknowledges financial support from the Fonds FCAR (Gouvernement du Québec). This work was made possible by a grant of computer time on a CRAY C98 supercomputer from the Institut du Développement et des Ressources en Informatique Scientifique under Projects Nos. 970425 and 980425.

[1] *Molecules in Laser Fields*, edited by A. D. Bandrauk (Dekker, New York, 1994).

[2] D. Normand, L. A. Lompré, and C. Cornaggia, *J. Phys. B* **25**, L497 (1992).

[3] A. D. Bandrauk and M. L. Sink, *J. Chem. Phys.* **74**, 1110 (1981).

[4] C. M. Dion, S. Chelkowski, A. D. Bandrauk, H. Umeda, and Y. Fujimura, *J. Chem. Phys.* **105**, 9083 (1996).

- [5] H. J. Loesch and A. Remscheid, *J. Chem. Phys.* **93**, 4779 (1990).
- [6] A. H. Zewail, *J. Chem. Soc., Faraday Trans. 2* **85**, 1221 (1989).
- [7] E. Charron, A. Giusti-Suzor, and F. H. Mies, *Phys. Rev. A* **49**, R641 (1994).
- [8] E. E. Aubanel and A. D. Bandrauk, *Chem. Phys. Lett.* **229**, 169 (1994).
- [9] A. D. Bandrauk and E. E. Aubanel, *Chem. Phys.* **198**, 159 (1995).
- [10] B. Friedrich and D. Herschbach, *Phys. Rev. Lett.* **74**, 4623 (1995).
- [11] T. Seideman, *J. Chem. Phys.* **106**, 2881 (1997); *Phys. Rev. A* **56**, R17 (1997).
- [12] H. Stapelfeldt, H. Sakai, E. Constant, and P. B. Corkum, *Phys. Rev. Lett.* **79**, 2787 (1997).
- [13] R. Numico, A. Keller, and O. Atabek, *Phys. Rev. A* **52**, 1298 (1995).
- [14] B. Friedrich and D. Herschbach, *J. Phys. Chem.* **99**, 15 686 (1995).
- [15] T. Seideman, *J. Chem. Phys.* **103**, 7887 (1995).
- [16] A. G. Maki, *J. Mol. Spectrosc.* **58**, 308 (1975).
- [17] A. D. Buckingham, *Adv. Chem. Phys.* **12**, 107 (1967).
- [18] H. Umeda, M. Sugawara, Y. Fujimura, and S. Koseki, *Chem. Phys. Lett.* **229**, 233 (1994).
- [19] H. Umeda and Y. Fujimura (private communication).
- [20] J. M. Bowman, B. Gazdy, J. A. Bentley, T. J. Lee, and C. E. Dateo, *J. Chem. Phys.* **99**, 308 (1993).
- [21] M. D. Feit, J. A. Fleck, Jr., and A. Steiger, *J. Comput. Phys.* **47**, 412 (1982).
- [22] A. D. Bandrauk and H. Shen, *J. Chem. Phys.* **99**, 1185 (1993).
- [23] C. E. Dateo and H. Metiu, *J. Chem. Phys.* **95**, 7392 (1991).
- [24] B. Yang, K. J. Schafer, B. Walker, K. C. Kulander, P. Agostini, and L. F. DiMauro, *Phys. Rev. Lett.* **71**, 3770 (1993).
- [25] P. Dietrich, P. B. Corkum, D. T. Strickland, and M. Laberge, in *Molecules in Laser Fields*, edited by A. D. Bandrauk (Dekker, New York, 1994), Chap. 4.
- [26] M. J. DeWitt and R. J. Lewis, *J. Chem. Phys.* **102**, 8670 (1995).
- [27] *CRC Handbook of Chemistry and Physics*, 77th ed., edited by D. R. Lide (CRC, Boca Raton, FL, 1996).
- [28] L. F. DiMauro (private communication).
- [29] L. D. Landau and E. M. Lifshitz, *Mechanics* (Pergamon, Oxford, 1960), Sec. 30.
- [30] The exact dynamical alignment time from an angle θ_0 close to $\pi/2$ to $\theta=0$, given by one-fourth of the period of the $\Theta(t)$ motion, can be calculated by integration of Eq. (27) and is $\tau/4 = \Omega^{-1} K(\sin\theta_0)$, with K an elliptic integral of the first kind.
- [31] G. Herzberg, *Molecular Spectra and Molecular Structure II. Infrared and Raman Spectra of Polyatomic Molecules* (Van Nostrand, Princeton, 1945).
- [32] M. J. J. Vrakking and S. Stolte, *Chem. Phys. Lett.* **271**, 209 (1997).
- [33] S. Chelkowski, A. D. Bandrauk, and P. B. Corkum, *Phys. Rev. Lett.* **65**, 2355 (1990).
- [34] P. Brumer and M. Shapiro, in *Molecules in Laser Fields*, edited by A. D. Bandrauk (Dekker, New York, 1994), Chap. 6.